Supporting information

Understanding the Li-Ion Storage Mechanism in a Carbon Composited Zinc Sulfide Electrode

Guiying Tian[a, †], Zijian Zhao[a, †], Angelina Sarapulova[a], Chittaranjan Das[a], Lihua Zhu[a], Suya Liu[b, c], Aleksandr Missiul[d], Edmund Welter[e], Julia Maibach[a], and Sonia Dsoke[a, f *]

[a]Institute for Applied Materials (IAM), Karlsruhe Institute of Technology (KIT), Hermann-von-Helmholtz-Platz 1, 76344 Eggenstein-Leopoldshafen, Germany

[b]International Center for New-Structured Materials (ICNSM), Zhejiang University (ZJU), 310027, Zheda Rd 38, Hangzhou, P.R. China

[c]Institute of Nanotechnology (INT), Karlsruhe Institute of Technology (KIT), Hermann-von-Helmholtz-Platz 1, 76344 Eggenstein-Leopoldshafen, Germany

[d]CELLS-ALBA, Carrer de la Llum 2-26, 08290 Cerdanyola del Vallès, Barcelona, Spain[e]Deutsches Elektronen-Synchrotron DESY, Notkestrasse 85, D-22607 Hamburg, Germany

[f]Helmholtz-Institute Ulm for Electrochemical Energy Storage (HIU), Helmholtzstrasse 11, 89081 Ulm, Germany

[*] Corresponding author: Tel.:+49 721 608 41915 *E-mail address*: sonia.dsoke@kit.edu (S. Dsoke)

[†] G. Tian and Z. Zhao contributed equally to this work

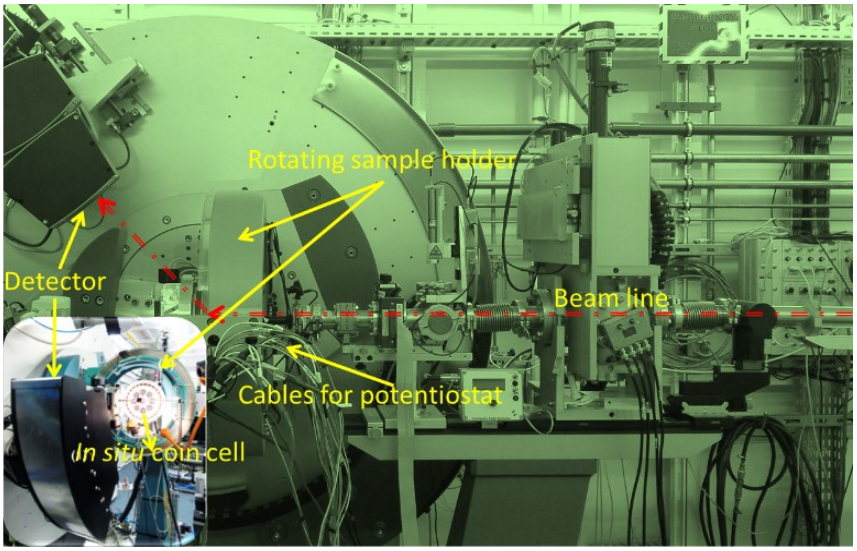

Fig. S1 Overview of the *in situ* SRD instruments at MSPD, ALBA.

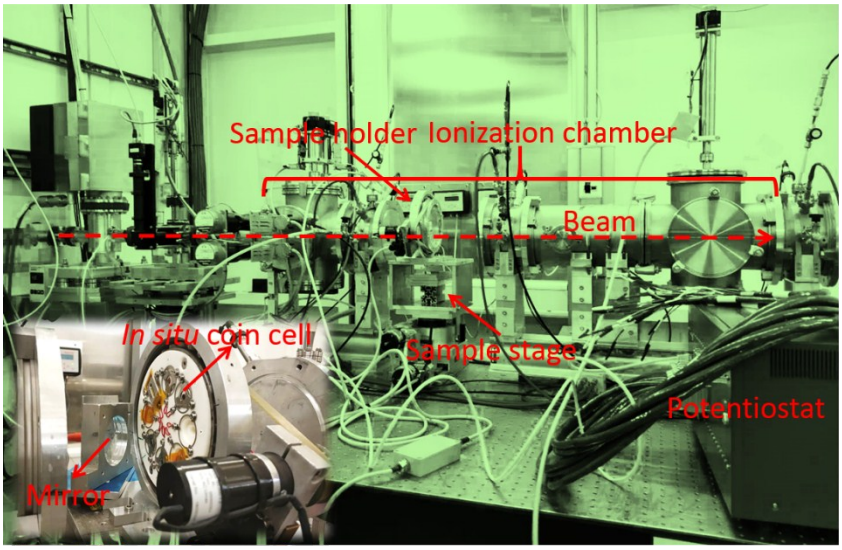

Fig. S2 Overview of the *in situ* XAS beamline at P65, PETRA III, DESY.

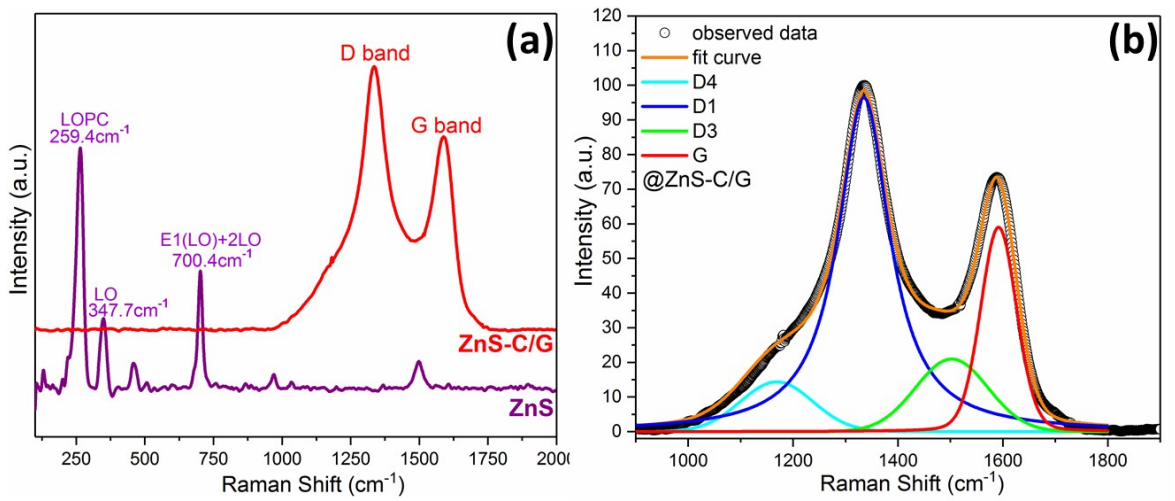

Fig. S3. (a) Raman spectra (λ = 632 nm) of the ZnS and ZnS-C/G composite, and (b) the curve fitting of the ZnS-C/G composite.

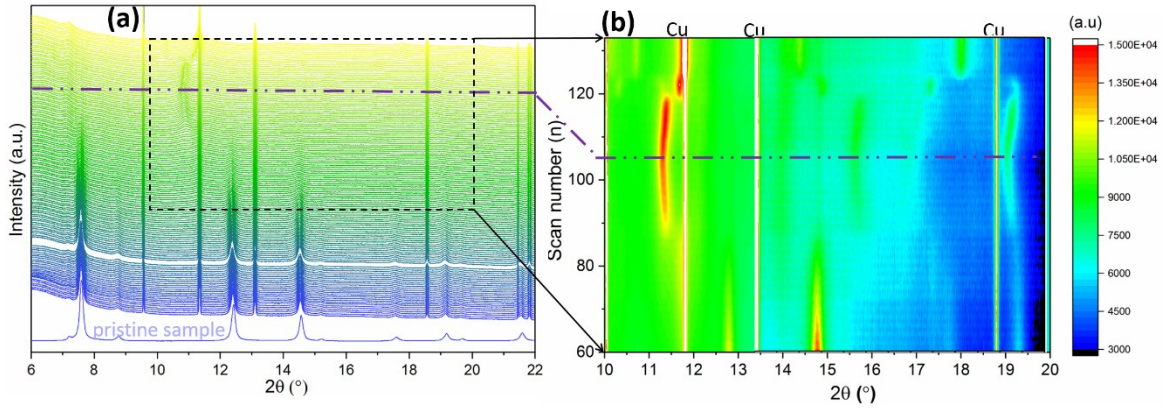

Fig. S4. (a) Waterfall plot of the total SRD patterns for a clear overview, and (b) contour map of the selected area in the SRD patterns to clearly display the change of intensity.

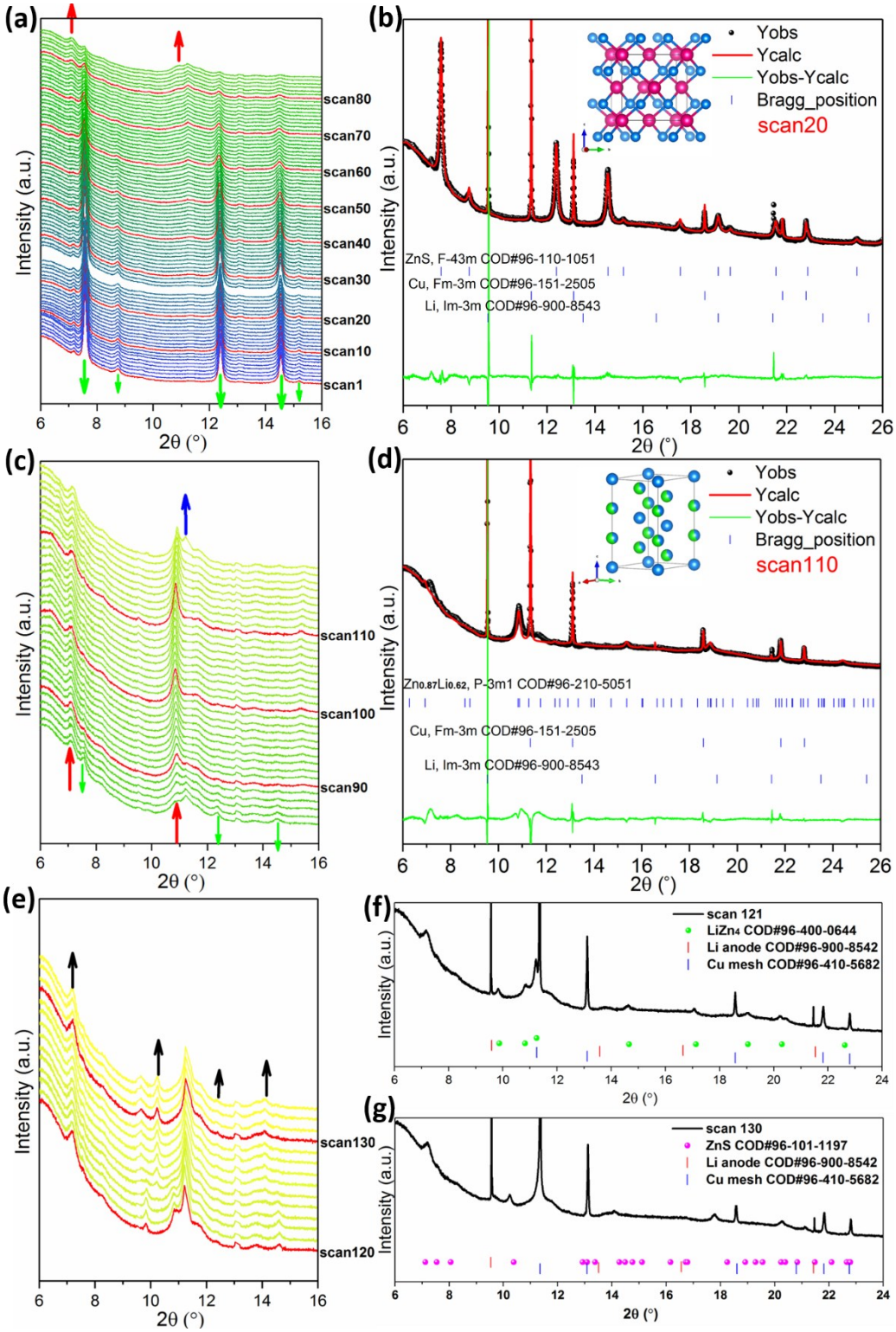

Fig. S5. Details of the structural evolution based on *in situ* SRD patterns: (a, b) step I, (c, d) step II+III and (e~g) step IV. Note: the reflections of copper current collector and lithium counter electrode are also shown.

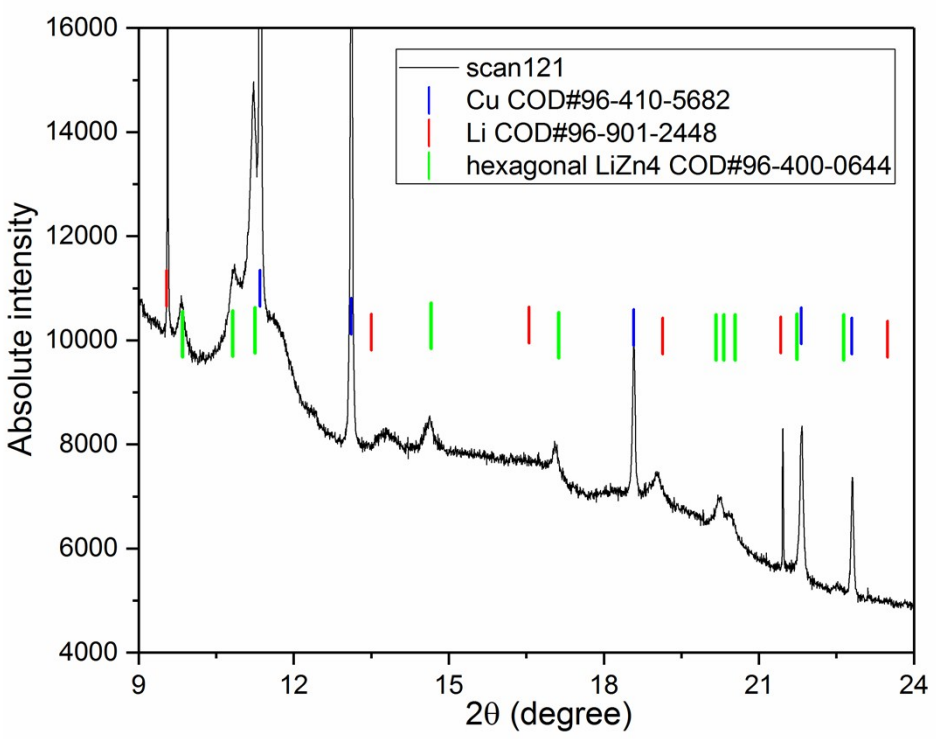

Fig. S6 Absolute intensity of the diffraction peaks of the scan121 and reference in the in situ XRD test.

Table S1. The potential and corresponding Zn contained phase composition obtained by linear combination fitting at varying scan points during the 1st lithiation.

scan number	potential (V)	Zn (wt.%)	ZnS (wt.%)
pristine	1.854	0	100
scan1	0.447	3.7	96.3
scan2	0.401	8.6	91.4
scan3	0.355	12.3	87.7
scan4	0.316	12.3	87.7
scan5	0.280	15.5	84.5
scan6	0.249	18.8	81.2
scan7	0.218	24.8	75.2
scan8	0.188	32.7	67.3
scan9	0.152	44.1	55.9
scan10	0.117	54.9	45.1
scan11	0.074	67.2	32.8
scan12	0.049	68.4	31.6

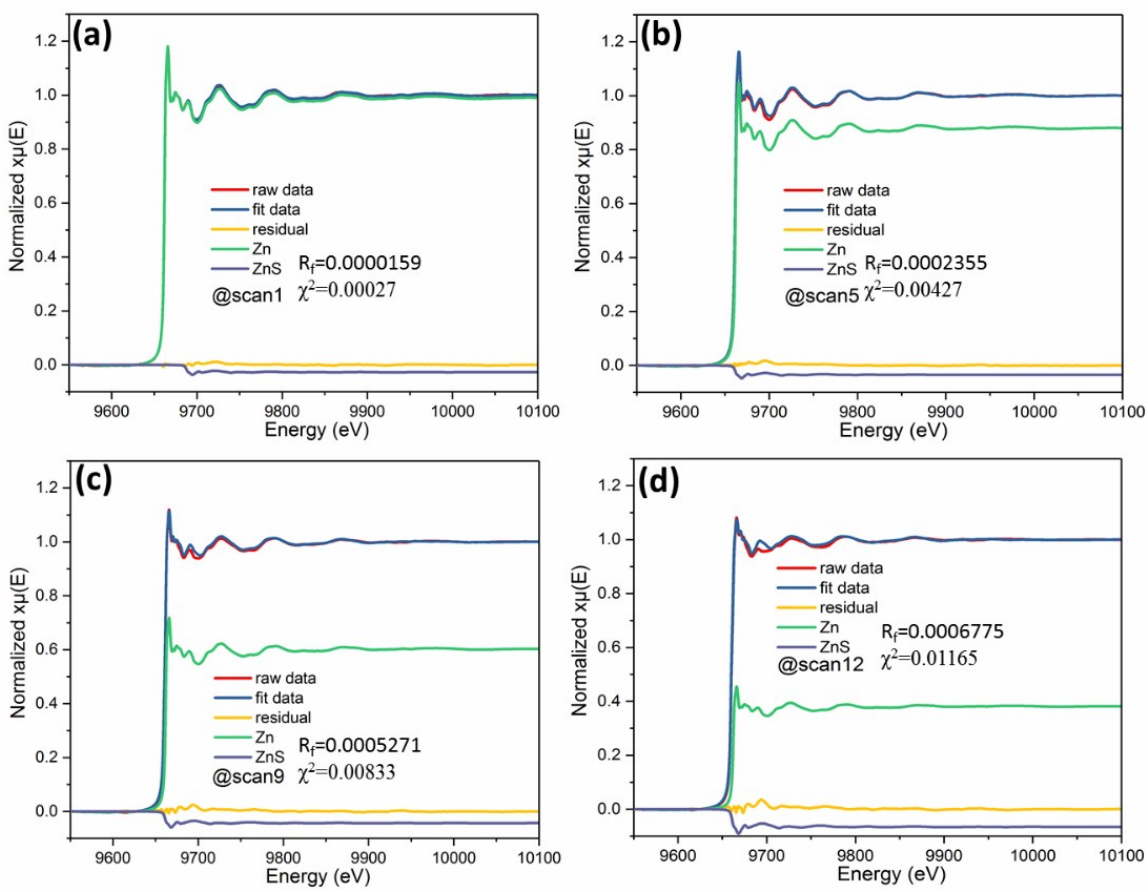

Fig. S7 Linear combination fitting of the XANES spectra at scan1, scan5, scan9 and scan12.

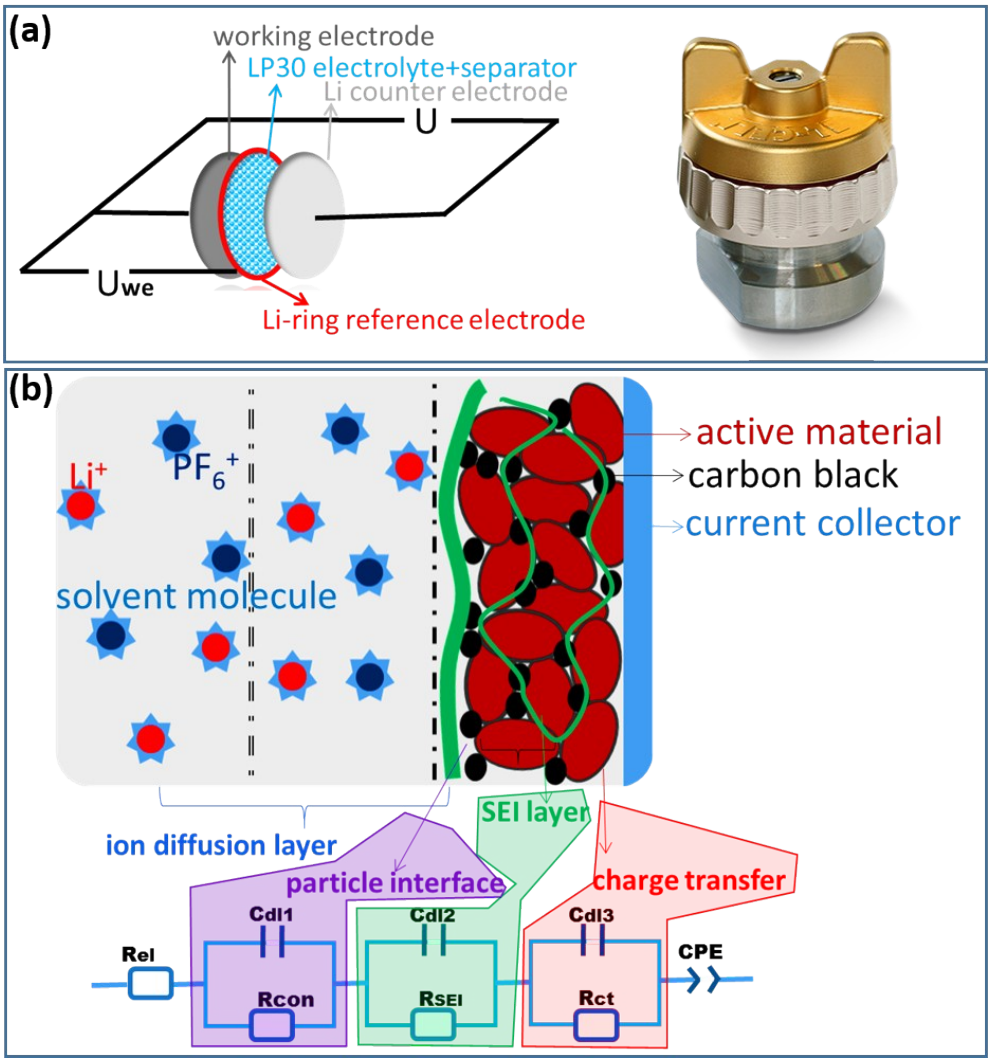

Fig. S8 (a) The schematic illustration and digital image of the three electrode EL-CELL® cell; (b) illustration of equivalent circuit for fitting the Nyquist plots.

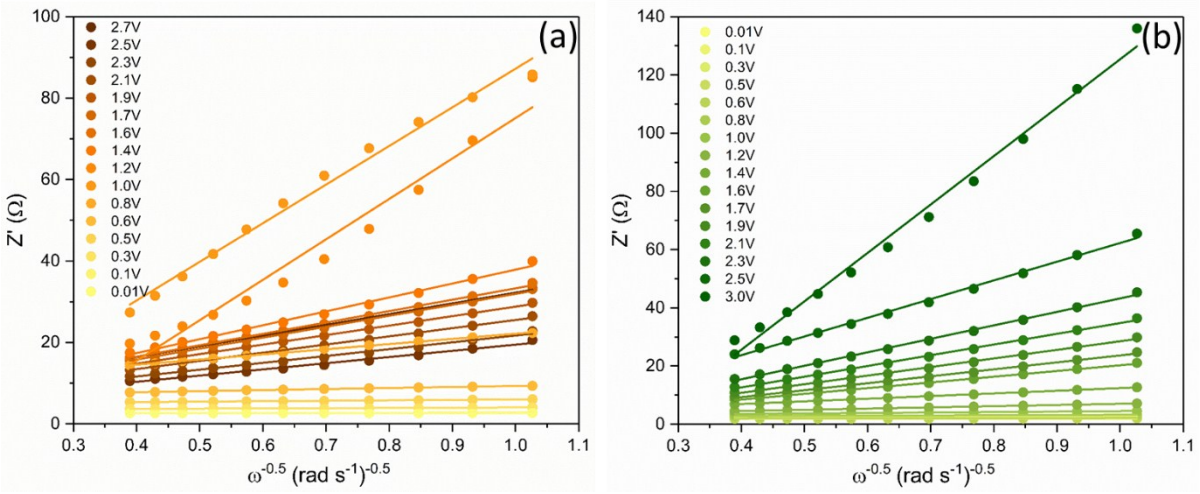

Fig. S9 The plots of the real part of impedance (Z') as a function of the inverse square root of angular frequency ($\omega^{-0.5}$) at lithiated (a) and delithiated (b) states for the ZnS-C/G electrode in the Warburg region.

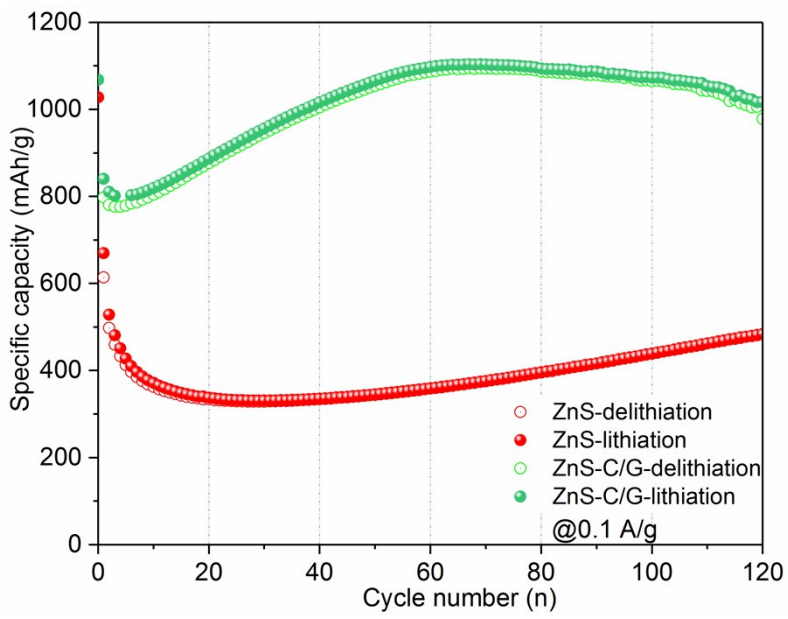

Fig. S10 Long-term cycling capacity at current density of 0.1 A g^{-1} with a potential window of 0.01~3.0 V.

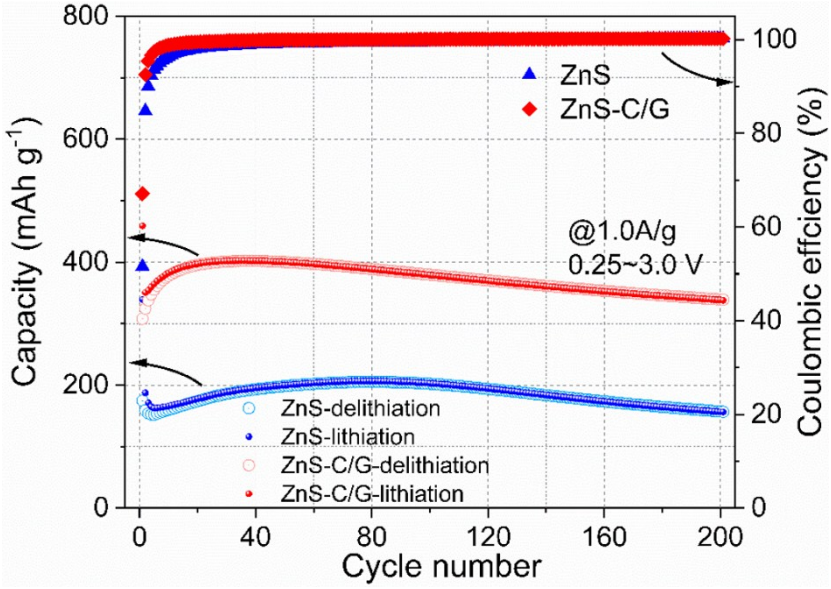

Fig. S11 Long-term cycling capacity at current density of 1.0 A g^{-1} with a potential window of 0.25~3.0 V.

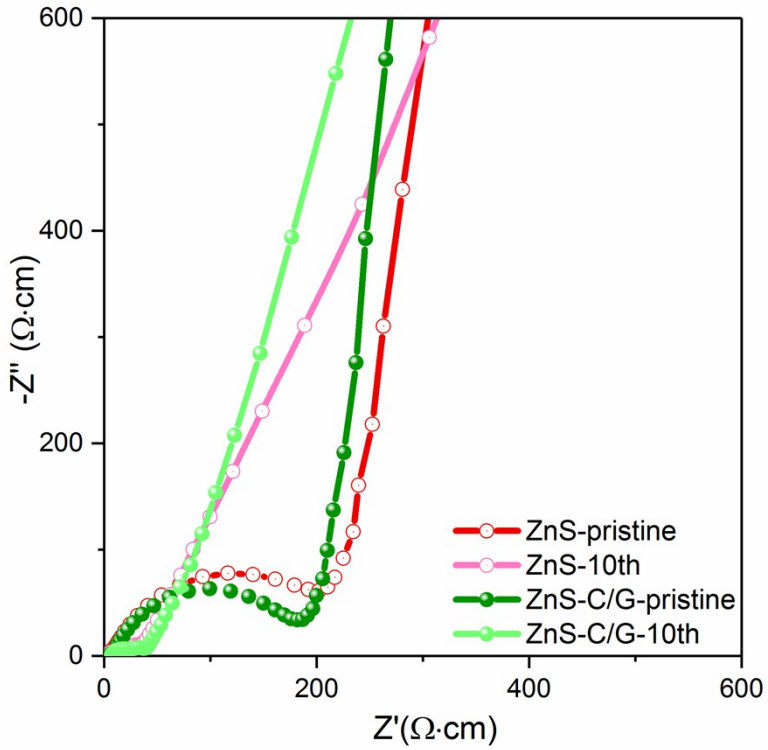

Fig. S12 Nyquist plots recorded at the delithiated state of the pristine electrodes and the electrodes after ten cycles for the ZnS and the ZnS-C/G.